Journal of Environmental Chemical Engineering 11 (2023) 110618

Contents lists available at ScienceDirect

Journal of Environmental Chemical Engineering

journal homepage: www.elsevier.com/locate/jece

Can tundish deskulling waste be used as a magnesium oxide source to develop magnesium phosphate cement?

A. Alfocea-Roig [a], S. Huete-Hernández [a], Í.X. García-Zubiri [b], J. Giro-Paloma [a], J. Formosa [a,*]

[a] Departament de Ciència de Materials i Química Física, Universitat de Barcelona, Martí i Franquès 1-11, 08028 Barcelona, Spain
[b] Magnesitas Navarras, S.A., Av. Roncesvalles, 31630 Zubiri, Spain

ARTICLE INFO

Editor: Apostolos Giannis

Keywords:
Circular economy
Refractory waste
Magnesium phosphate cement
Steel industry waste
Valorisation

ABSTRACT

Ordinary Portland cement (OPC) has a significant environmental impact since approximately 0.81 kg of CO_2 is generated for every kilogram produced. Thus, it is mandatory to look for sustainable alternative cements. One of the most promising materials in this sense is magnesium phosphate cement (MPC). This study evaluates the possibility of revaluing a waste obtained from the tundish deskulling (TUN) as a raw material for formulating alternative MPC. This approach aims to promote the circular economy and minimizing the environmental impact of MPC. The tundish working lining is a crucial refractory material used in continuous steel casting. An optimal cement formulation was achieved by maximizing the compressive strength (CS) at 7 days, resulting in the combination of 60 wt% of TUN and 40 wt% of KH_2PO_4, with a water/cement (W/C) ratio of 0.27. The physical and mechanical properties were evaluated at three different stages: after 1, 7, and 28 days of curing. Furthermore, an exhaustive physicochemical characterization was conducted to investigate the feasibility of using it as an alternative cement. This study confirms the feasibility of formulating MPC using TUN as raw material due to the main product obtained, which is K-struvite. The use of TUN implies important economic savings and enhances sustainability criteria avoiding its management in landfills.

1. Introduction

The Industry current new lines of research are mainly focused on the circular economy, energy efficiency, and greenhouse gas (GHG) emissions reduction. Primary resources from mining activities remain a significant prerequisite to appease the growing global demand for raw materials. Hence, mining is crucial, even more so in a circular economy tendency. Improving the production processes and product design of a product can minimise the amount and volume of the demanded raw materials. More efficient reuse, repair, and recycling of waste and by-products can be accomplished. In this sense, it is necessary to continue studying for better efficiency in mining operations to achieve the goal of zero waste mining, using secondary resources from mine waste to its fullest potential.

The steel industry is the largest consumer of refractory materials (about 70 %). The refractory materials are divided into two types: unshaped (monolithic refractories) with 45 % and shaped refractories with 55 % [1]. These are classified by their chemical composition, density, or type of blend [2,3]. Specifically, non-shaped includes also refractories made of magnesia (47 %). Following a study on critical raw materials in the EU in 2020, it is estimated that 57 % of EU magnesite consumption comes from steelmaking [4]. These refractories are used in this industry as they exhibit high temperature resistance (> 1500 ºC), slag resistance, and chemical and physical resistance to molten metals.

The highest consumption (42 %) of refractories in steelmaking corresponds to the tundish masses coating [5]. Tundish is an essential component for the process of continuous casting of steel, as it is the last container with refractory material to deliver molten metal at a controlled speed to the moulds [6]. Fig. 1. A shows the process of steel production and Fig. 1. B shows the container before its use. The functions of the container include smoothing the outflow, regulating the feeding of the metal to the moulds, and cleaning the metal, among other operations. For this reason, the refractories in the container must be renewed periodically since the slag generated in the process can interfere with them, therefore, making them less effective. The service lifetime of the tundish masses depends on the service conditions and the

Abbreviations: MPCs, Magnesium phosphate cements; MKP, Monopotassium phosphate; OPC, Ordinary portland cement; MKPC, Magnesium potassium phosphate cement; TUN, Tundish deskulling waste; MPC-TUN, Magnesium phosphate cement - Tundish deskulling waste.

* Corresponding author.
E-mail address: joanformosa@ub.edu (J. Formosa).

https://doi.org/10.1016/j.jece.2023.110618
Received 11 May 2023; Received in revised form 30 June 2023; Accepted 20 July 2023
Available online 22 July 2023

Fig. 1. A (right). Scheme of steel production which the number 2 is related to the Tundish container. B (left). Tundish based on MgO refractory container (supplied by Magnesitas Navarras, S.A.).

performance of the material, but once it exceeds the quality and safety conditions, the masses are replaced with new material. Therefore, a high amount of waste is generated, containing significant impurities, and being difficult to separate and recycle. This waste is known as tundish deskulling (TUN).

The raw materials demand for the manufacture of refractory materials is only covered with 5–8 % of recycled materials, which is approximately 2.5 million tons [1,7]. The utilization of TUN as a raw material after its service life enables a reduction in the extraction of new minerals, water pollution, waste associated with mineral extraction, and ground degradation. Hence, this leads to a reduction in the environmental impact associated. The EU Directive on the landfill of waste (Directive 2018/850) classifies landfill sites into three different types: inert waste, hazardous waste and, non-hazardous waste [8]. Refractories are considered non-hazardous waste, and the Directive establishes targets to introduce restrictions on landfilling. The objective of the European Parliament is to incentivize the circular economy and waste management. In that regard, the valorization of TUN can contribute to the achievement of various goals outlined in Directive 2008/98/EC on waste and Directive 1999/31/EC on the landfilling of waste [8,9].

As abovementioned, the primary sector driving the demand for magnesia globally is the steel industry, but the cement sector also plays a significant role [4]. Hence, it is important to seek for new applications for magnesia refractory waste. Consequently, TUN could be a sustainable alternative to the raw materials traditionally employed for developing Magnesium Phosphate Cement (MPC), which has a high potential to reduce the use of Ordinary Portland Cement (OPC) in some applications, such as for example in precast cements, repair cements, among others. OPC is one of the most manufactured materials in the world [10]. The OPC industry emits around 7 % of global anthropogenic CO_2 emissions and it is the third-largest industrial energy consumer [3]. This is attributed to the calcination of raw materials that leads to the formation and release of CO_2, as well as the high energy demand to maintain high temperatures in the clinkerization process. To manufacture 1 ton of OPC, approximately 900 kg CO_2 is emitted, and 1.5 tons of raw material are required [11]. Therefore, the scientific and technological community is looking for alternative types of cement to reduce GHG emissions, energy demand, and consumption of natural resources from the manufacture of cement. The challenges faced by industries include the utilization of alternative fuels instead of conventional fossil fuels and partially substituting clinker with waste or industrial by-products. The implementation of these solutions can contribute to the achievement of Sustainable Development Goals (SDG) and reducing CO_2 levels and other GHG emissions in the atmosphere, among other challenges [12,13].

MPCs are hydraulic cements that are formed through an acid-base reaction. In particular, the reaction between MgO and monopotassium phosphate (KH_2PO_4, MKP) in an aqueous solution at room temperature leads to the formation of magnesium potassium phosphate cement (MKPC), with $MgKPO_4{\cdot}6H_2O$, also known as K-struvite, as the main reaction product, as shown in Eq. (1) [14,15].

$$MgO_{(s)} + KH_2PO_{4(s)} + 5H_2O \xrightarrow{(l)} MgKPO_4{\cdot}6H_2O_{(s)} \quad (1)$$

MPCs have several advantages such as neutral pH, low water demand, fast setting, high early strength, good waste encapsulation, and low drying shrinkage, among others features [16–18]. Due to these properties, the applications of MPCs are highly diverse as they have been extensively used as a repair and reinforcement cements in civil engineering, as stabilizers/solidifiers of radioactive waste, and in biomedical applications [15–20].

The objective of this study is to assess the potential of using TUN, which is defined as tundish deskulling waste, as a MgO source for developing an alternative magnesium phosphate cement; named as MPC-TUN. The assessment of its potential was conducted from various perspectives, including morphological, physical, chemical, environmental, and mechanical viewpoints. Different formulations were

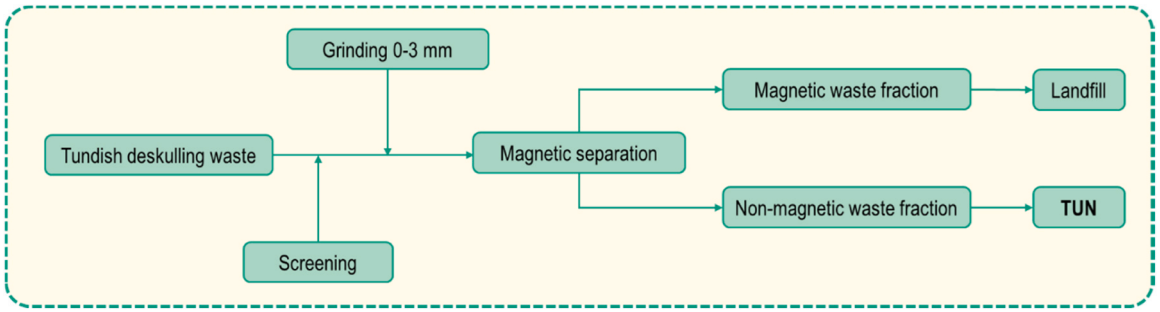

Fig. 2. Conditioning of TUN.

performed by maximizing the compressive strength (CS) at 7 days. The resultant optimal formulation was characterized at 1, 7, and 28 days of curing. In addition, it should be noted that this alternative material can reduce the CO_2 emissions, energy demand, and resource consumption by following the challenges and agreements set internationally, such as the Paris Agreement. In addition, the MPC-TUN alternative cement contributes positively to the challenge of carbon neutral concrete in 2050 [21].

2. Materials and methods

2.1. Materials

TUN was supplied by Magnesitas Navarras, S.A. company (Navarra, Spain). It originates from a Basauri steel mill, located in Bizkaia (Spain), which has an annual steel production of approximately 700 kt and consumes 2.7 kt of tundish masses [22]. After its recollection, it has to be screened, milled (to obtain a particle size below 3 mm) and subsequently demagnetized (to remove magnetic impurities from the slag), as shown in Fig. 2. On one hand, various wastes are generated during the conditioning process, primarily from screening and grinding operations, which are subsequently disposed of in landfills, accounting for 22.46 % of the total waste. Additionally, the magnetic waste fraction (13.66 %) is also disposed of in landfills. On the other hand, the TUN utilized as a raw material in this study comprises solely the non-magnetic fraction (63.88 %) of the original waste material. At the end of the conditioning process, the non-magnetic fraction is quartered and homogenized to obtain a representative chemical composition.

The phosphate source was KH_2PO_4, known as MKP and was supplied by Norken, S.L. (food-grade, purity: 99.8 wt%). Boric acid (H_3BO_3, HB) was supplied by Borax España, S.A., is used as a setting retarder and to control thermal expansion [23].

2.2. TUN characterization

To characterize the chemical composition and to determine the content of the most stable oxides, X-ray fluorescence spectroscopy (XRF) was employed using a Philips PW 2400 sequential X-ray spectrometer. TUN was characterized by X-ray diffraction (XRD) using a PANalytical X'Pert PRO MPD alpha1 powder diffractometer, with $CuK\alpha_1$ radiation. The resulting diffraction pattern was analyzed using the X'Pert HighScore software, and the main mineral and crystalline phases were determined by referencing the PDF2 database. Moreover, thermogravimetric analysis with derivative thermogravimetry (TG/DTG) was conducted with a TA Instruments Q-600 SDT from 30° to 1400°C at a heating rate of 10 °C min^{-1} in air and nitrogen atmosphere with gas flow of 50 mL·min^{-1}.

Besides, Fourier transformed infrared spectroscopy in attenuated total reflectance mode (FTIR-ATR) was used by means of Spectrum Two™ equipment from Perkin Elmer to detect the symmetric and asymmetric stretching vibration bonds. A 32-scan average was collected with a resolution of 4 cm^{-1}.

The specific surface area (SSA) was evaluated using the Brunauer-Emmett-Teller (BET) model with a TriStar 3000 V6.04 A. The particle size distribution (PSD) was determined with a Beckman Coulter® LSTM 13 320 device with a universal liquid module. Citric acid reactivity test (CART) was performed to study the reactivity of magnesium oxide and, consequently, to classify TUN from high reactivity (< 60 s) to dead-burnt, i.e., low reactivity (> 900 s) [17]. During the test, 2 g of TUN was combined with 100 mL of a citric acid solution. The resulting mixture was stirred at 500 rpm·min^{-1} at 30 °C and monitored using a pH-meter from Hannah Instruments to determine the time necessary to achieve a pH of 9 [17].

Leaching tests to determine the environmental potential impact were performed following the EN 12457–2 standard. The leachates were subsequently analysed employing inductively coupled plasma mass spectrometry (ICP-MS) with the NexION 350D equipment from Perkin Elmer.

Finally, the microstructure of TUN was analysed using scanning electron microscopy (SEM) and energy-dispersive X-ray spectroscopy (EDS). The TUN sample was carbon-coated to evaluate the particle morphology and elemental composition. This analysis was conducted using the ESEM FEI Quanta 200 equipment.

Table 1
Compressive strength of the preliminary study of different formulations.

	TUN/MKP (MPa)					
W/C	**60/40**	±	**55/45**	±	**50/50**	±
0.25	31.87	2.77	30.00	2.68	31.89	4.58
0.27	35.32	2.31	27.17	3.12	25.32	5.82
0.29	29.30	1.63	28.87	0.15	23.41	3.77
0.31	26.42	1.43	23.55	2.30	22.84	2.53
0.33	24.03	0.79	23.16	0.87	19.81	0.42
0.35	22.30	3.56	21.63	3.22	21.70	2.02

2.3. Samples preparation

The methodology for preparing the MPC-TUN formulations was thoroughly followed to ensure that there were no alterations in the variables that could potentially impact the final properties of the cements. MPC-TUN formulations were prepared in two steps. Firstly, a preliminary study was conducted by preparing small batches of 200 g of solid (MKP and TUN) in order to determine the proper dosage for conducting this study. The preliminary study was focused on obtaining the maximum CS at 7 days of curing with the absence of efflorescence.

In the preliminary study, the TUN/MKP ratios ranged from 80/20–20/80, with a 10 wt% variation for each dosage. The water/cement (W/C) ratio was set at 0.20 and 0.30. For each preliminary dosage, three specimens measuring 2.5 × 2.5 × 2.5 cm^3 were evaluated. Better results were obtained within the TUN/MKP ratio range of 60/40 and 50/50. Subsequently, a more detailed study was conducted within this range, following the same procedure outlined in Table 1, but with a W/C ratio between 0.25 and 0.35. The aim was to determine the appropriate TUN/MKP and W/C ratios for evaluating the properties of the MPC-TUN. The dosages of 50/50 presented efflorescence; for this reason, they were discarded. As shown in Table 1, the 60/40 TUN/MKP formulations achieved higher CS after 7 days of curing compared to the 55/45 formulations with the same W/C ratio. Hence, the formulation with 60 wt% of TUN and 40 wt% of KH_2PO_4 with a W/C ratio of 0.27 was chosen for the further study of MPC-TUN.

It should be highlighted that to increase the workability of this formulation (TUN/MKP = 60/40, and W/C = 0.27) a new batch was prepared by adding 1 wt% of HB relative to the total of solids (TUN and MKP). As it is reported in the literature, HB acts as a setting retarder and improves the workability of the mixture [14]. Three new MPC-TUN batches of 2000 g each were prepared using the best dosage above mentioned to obtain a total of nine 16 × 4 × 4 cm^3 prismatic specimens.

One important characteristic of MPCs, as mentioned earlier, is their ability to develop early strength, resulting in rapid setting. Consequently, a low final setting time is expected for MPC-TUN. The results of VICAT testing, following the UNE-EN 196–3 standard, reveal that the initial setting time is 3150 s, and the final setting time is 3690 s. This MPC-TUN formulation was prepared as it is shown Fig. 3. The solid cement components (i.e.: TUN, MKP, and HB) and the kneading water were weighed separately. Subsequently, the solid cement components were poured and homogenized for 60 s at low speed in a planetary mortar mixer. Then, the kneading water was added and the mixture was mixed during 180 s. The fresh mixture was moulded in three 16 × 4×4 cm^3 moulds, and cured in laboratory conditions. After 24 h of curing, the samples were demoulded. Then, the samples were cured up

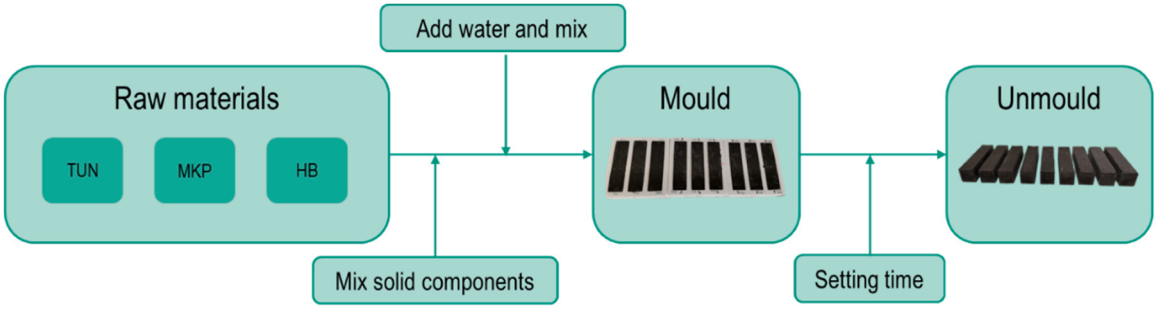

Fig. 3. Methodology to formulate the MPC-TUN.

Table 2
Characterization of TUN and MPC-TUN.

Techniques	TUN	MPC-TUN		
		Day 1	Day 7	Day 28
BET	✓	-	-	-
CART	✓	-	-	-
CS	-	✓	✓	✓
FS	-	✓	✓	✓
FT-IR	✓	-	-	✓
Leaching test	✓	-	-	✓
PSD	✓	-	-	-
SEM	✓	-	-	✓
TG/DTG	✓	-	-	✓
XRD	✓	-	-	✓
XRF	✓	-	-	-

to for 1, 7, and 28 days at room temperature under the same conditions. In total nine prismatic samples were performed, three per each specific cured time. The laboratory conditions (25 °C ± 1 °C and 50 % ± 5 % relative humidity) were kept constant during the experimental process. Finally, the samples were tested and analysed to evaluate the different physical, chemical, mechanical, and environmental properties.

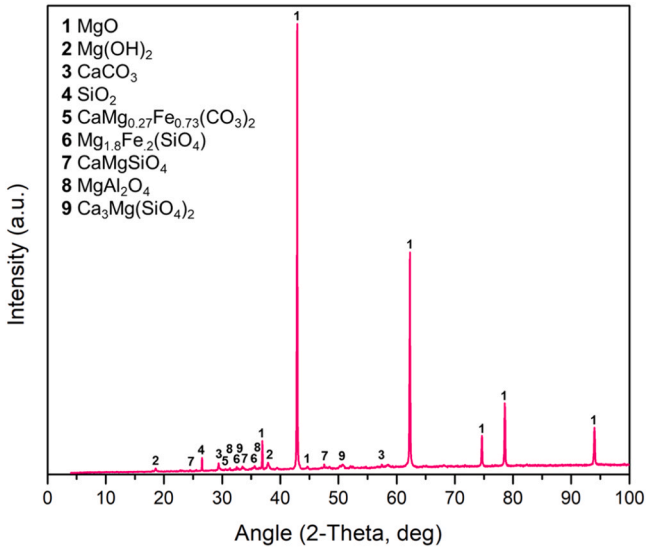

Fig. 4. XRD pattern of TUN.

2.4. Characterization of the MPC-TUN formulation

MPC-TUN formulation was characterized to determine physical, mechanical, chemical, and leaching properties, as shown in Table 2. The flexural strength (FS) and CS were evaluated with an Incotecnic MULTI-R1 universal testing machine, equipped with a 200 kN load cell, following the UNE-EN 196–1 standard. The FS and CS test speed was 5 kg·s^{-1} and 240 kg·s^{-1}, respectively. Apparent density following EN1936:2006, FS, and CS were evaluated at 1, 7, and 28 days of curing. On the other hand, the samples corresponding to the batch of 28 days of curing were thoroughly analysed by means of XRD, TG/DTG, FT-IR, BET, leaching test, and SEM-EDS.

In this regard, XRD analysis was performed using a Bragg-Brentano Siemens D-500 powder diffractometer with CuKα1 radiation. The resulting diffraction pattern was interpreted using the X'Pert HighScore software, with reference to the PDF2 database, to analyse the main crystalline phases of the MPC-TUN reaction products.

The TG/DTG analysis was performed using the same equipment employed for the characterization of raw materials. The analysis was performed in both air and nitrogen atmospheres (at a flow rate of 50 mL·min^{-1}) with a heating rate of 10 °C·min^{-1} up to 1400 °C. Furthermore, FTIR-ATR was conducted in the same conditions as TUN was analysed to determine the atomic bonds vibrations in order to understand more the chemical structure of MPC-TUN. The potential release of heavy metals and metalloids was assessed according to the EN 12457–2 standard, which enabled the simulation of leaching behaviour after the service lifetime of the material. MPC-TUN was crushed below 4 mm following the UNE-EN 12457–2. The leaching procedure involves the extraction heavy metals from the solids using deionized water with a liquid-to-solid ratio of 10 L·kg^{-1}. This extraction process was conducted for 24 h under continuous stirring at 10 rpm and at room temperature. Subsequently, the leachate was separated and filtered using a 0.45 mm pore membrane, and analysed by means of ICP-MS with the NexION 350D Perkin Elmer equipment. The following elements were evaluated, as specified by the standard: As, Ba, Cd, Cr, Cu, Hg, Mo, Ni, Pb, Sb, Se, V, and Zn.

Finally, the microstructure and morphology of the samples were characterized through SEM using ESEM FEI Quanta 200 equipment. Backscattered electron images were collected and combined with EDS elemental mapping (20 kV, working distance of 15 mm) to obtain high contrast micrographs, where each colour corresponds to the different elemental composition found in the sample. SEM-EDS was used to determine the elemental composition in different areas of the developed MPC-TUN samples after 28 days of curing. The fragments of MPC-TUN

Table 3
XRF analysis of TUN expressed in wt%.

Compounds	MgO	CaO	SiO_2	Al_2O_3	Fe_2O_3	SO_3	P_2O_5	Cr_2O_3	Na_2O	LOI
wt%	68.70	9.43	8.67	4.68	3.56	0.15	0.11	0.07	0.02	4.61

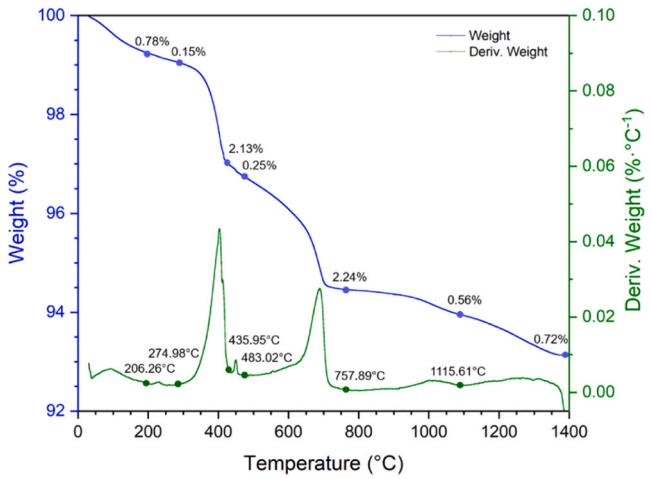

Fig. 5. TG/DTG of TUN.

were fixed on a carbon adhesive and carbon-coated. Additionally, polished samples were examined to reveal the internal structure of the MPC-TUN matrix and embedded particles.

3. Results and discussion

3.1. Raw material characterization

The chemical composition of TUN determined by XRF is shown in Table 3 as the most stable oxide for each element. As expected, the most abundant element is magnesium, with an average MgO content of 68.70 wt%. Following MgO, the most abundant elements are calcium, silicon, aluminium, and iron as CaO (9.43 wt%), SiO_2 (8.66 wt%), Al_2O_3 (4.68 wt%), and Fe_2O_3 (3.56 wt%), respectively. The Loss on Ignition (LOI) refers to the mass loss up to 1050 °C, resulting in 4.61 wt%.

Fig. 4 presents the XRD pattern of TUN, indicating the primary crystalline phases, which are magnesium oxide (MgO, 01-078-0430), brucite ($Mg(OH)_2$, 01-082-2453), and calcite ($CaCO_3$, 01-083-0578). In addition, other crystalline phases are compatible with the following phases: silicon oxide (SiO_2, 01-081-0065), ankerite ($CaMg_{0.27}Fe_{0.73}(CO_3)_2$, 01-084-2067), forsterite ($Mg_{1.8}Fe_{0.2}(SiO_4)$, 01-079-2184), monticellite ($CaMgSiO_4$, 01-084-1321), spinel ($MgAl_2O_4$, 01-077-0436), and merwinite ($Ca_3Mg(SiO_4)_2$, 01-074-0382).

The TG/DTG analysis showed a total mass loss of 6.82 wt% in N_2 atmosphere when heated from 30 ºC to 1400 ºC. Seven different mass losses are shown in Fig. 5 (blue dots), as well as the temperature range of each one (green dots). The first step is related to water loss due to the moisture of the sample from 30 ºC to 206 ºC (0.78 wt%). The following decompositions are from 206 ºC to 275 ºC (0.15 wt%, not assigned), from 275 ºC to 436 ºC (2.13 wt%) due to the $Mg(OH)_2$ decomposition, as well as $Ca(OH)_2$ decomposition from 436 ºC to 483 ºC (0.25 wt%). The following two decompositions are assigned to two different carbonates decomposition (ankerite and calcite, respectively) from 483 ºC to 1116 ºC (2.8 wt%), and the last loss up to 1400 ºC (0.72 wt%) is attributed to sulphates, which is probably due to the presence of $CaSO_4$ in TUN, and it could be also related to the not assigned weight loss from 206 to 275 ºC.

The TG/DTG results in combination with the XRD and XRF results were used to estimate the chemical composition of TUN, as shown in Table 4. The TG/DTG results allow an approximate percentage of compounds that decomposed thermally up to 1400 ºC, the XRF results were used to calculate the remaining composition, and finally, the XRD results enables the recognition of the chemical compounds that were decomposed thermally during the TG/DTG tests. Although the presence of sulphates is not determined by XRD (see Fig. 4), its presence is interpreted in the previous TG/DTG analysis with a weight loss of 0.723 % above 1100 °C (see Fig. 5). The TUN analysis results point out that the main compound obtained is MgO. Besides, the presence of $Mg(OH)_2$ is attributed to a hydration process on the surface of MgO particles of TUN that occurs due to atmospheric exposure during the conditioning process. The presence of $Mg(OH)_2$ does not interfere with the development of MPC-TUN. The crystalline phases containing Si do not decompose below 1400 ºC, for this reason they are not indicated per separate in Table 4, included as other compounds (15.54 wt%) as well as the spinel phase determined by XRD (see Fig. 4).

Table 4
Estimated composition of TUN by means of XRD-TG/DTG-XRF.

Compounds	MgO	$Mg(OH)_2$	CaO	$CaMg_{0.27}Fe_{0.73}(CO_3)_2$	$CaSO_4$	$CaCO_3$	$Ca(OH)_2$	Others
wt%	61.42	6.90	6.05	5.27	2.51	1.27	1.04	15.54

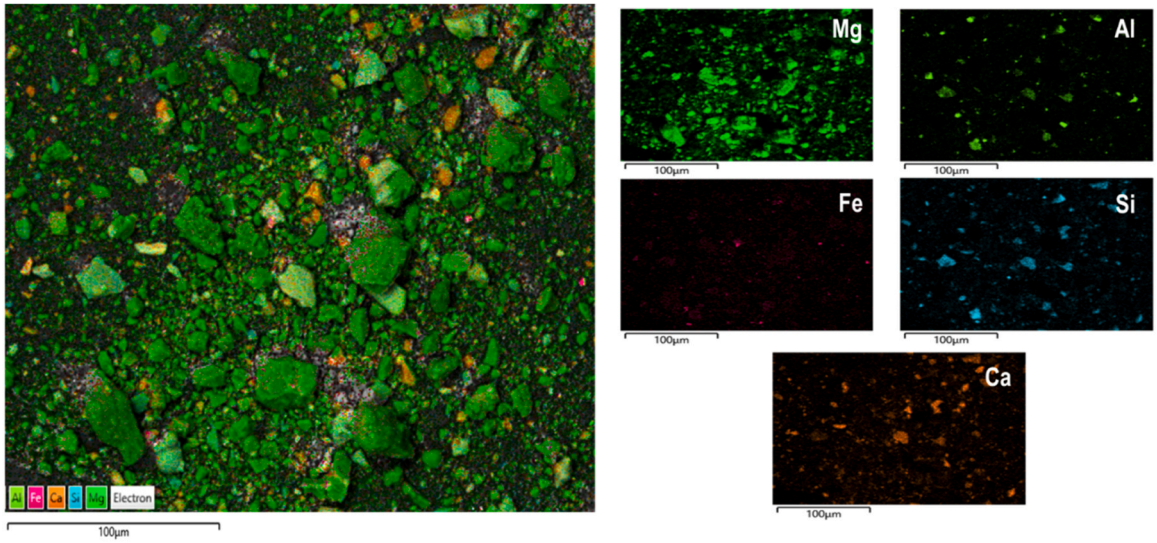

Fig. 6. SEM-EDS of TUN (x450). General elemental mapping (left) and the elemental mapping (right).

Table 5
Density values of MPC-TUN.

Fresh bulk density	Bulk density Day 7	Bulk density Day 28
	$kg \cdot m^{-3}$	
1920 ± 0.01	1840 ± 0.01	1760 ± 0.01

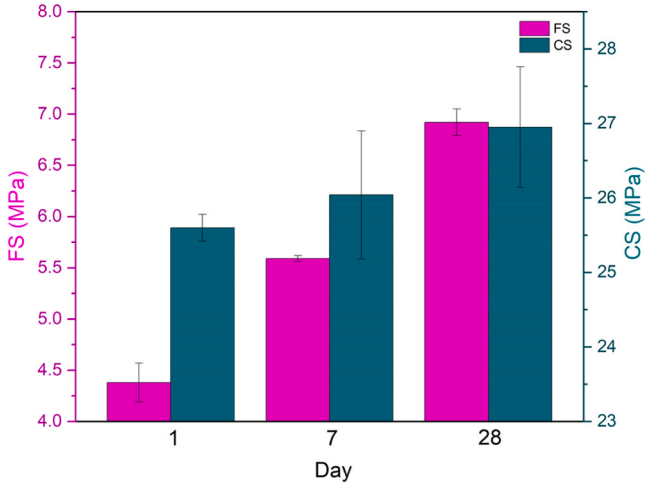

Fig. 7. Mechanical properties of MPC-TUN.

In addition, the SSA of the raw material was 3.57 $m^2 \cdot g^{-1}$. The SSA determined by BET analysis indicates that TUN exhibits a very low reactivity in terms of surface area. PSD analysis revealed that 10 % of particles (d_{10}), 50 % of particles (d_{50}), and 90 % of particles (d_{90}) were below 0.72 μm, 3.31 μm, and 7.85 μm, respectively. TUN CART result is greater than 900 s, which classifies the waste as dead-burned MgO, with low reactivity. Pure MgO exhibits high reactivity and tends to agglomerate when used in the development of MPC, resulting in poor workability of the paste and a non-homogeneous material. Therefore, pure MgO needs to undergo precalcination processes to obtain a suitable reactivity. However, the low reactivity of TUN, as far as we know, can be advantageous for the effective development of MPC. This characteristic helps minimize the environmental impact as it eliminates the need for precalcination, leading to a reduction in energy consumption during the manufacturing process [14].

Fig. 6 presents the SEM-EDS elemental mapping of TUN particles. The micrograph shows a high dispersion of particles with varying sizes, consistent with the results obtained from the PSD analysis. In addition, the particles present an angular shape due to the grinding process in the conditioning stage. In relation to elemental mapping, the main element is Mg, but it is also possible to observe others such as Al, Fe, Si, and Ca. These elements agree with the above-mentioned crystalline phases determined by XRD, mainly originating from silicon oxide, ankerite, forsterite, monticellite, spinel, and merwinite.

3.2. MPC-TUN characterization

The density values of MPC-TUN are shown in Table 5. As the curing time progresses, the density of TUN-MPC decreases, which is attributed to an increase in porosity resulting from the release of water during the drying process [24].

The mechanical characterization results, in terms of FS and CS of the formulation tested after 1, 7, and 28 days are shown in Fig. 7. An increasing trend in FS and CS results is observed with the curing time. The FS and the CS after 28 days of curing are approximately 7 and 27 MPa, respectively. It is essential to understand that the difference between the CS results of the preliminary study and the final formulation is due to the difference in sample size, as well as the shape of the

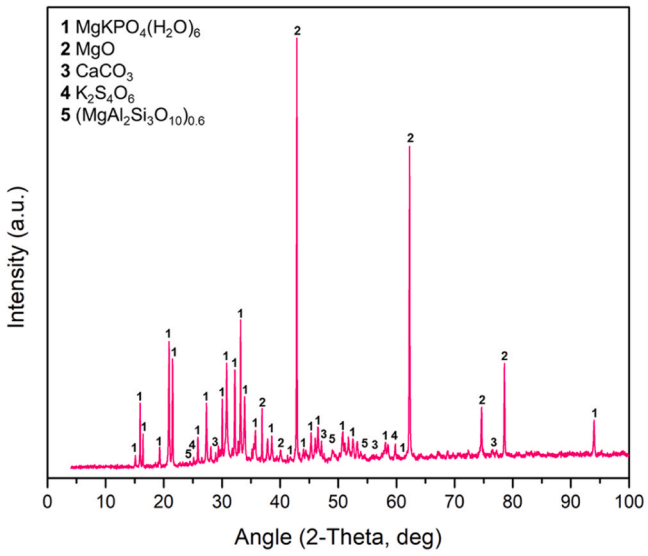

Fig. 8. XRD MPC-TUN.

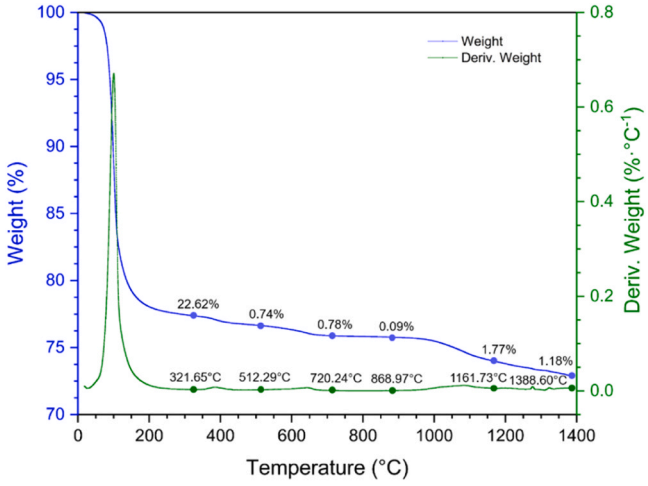

Fig. 9. TG/DTG MPC-TUN.

samples, which directly impact the results. It should be mentioned that as the curing days increase, both FS and CS results show higher values. However, the increase is more pronounced in the FS test compared to the CS test, which can be attributed to the nature of each test and the porosity of the samples. These findings are consistent with previously reported mechanical results for MPCs formulated with similar waste and/or by-products [25]. Other studies with different by-products of MgO, such as low-grade magnesium oxide (LG-MgO), achieved similar responses with same specimen size. These findings suggest that the use of LG-MgO and similar by-products could be relevant for specific construction applications [17].

The XRD results are shown in Fig. 8, which confirms that the K-struvite ($MgKPO_4(H_2O)_6$, 01-075-1076) is the majority phase, but also other minor phases, such as unreacted magnesium oxide (MgO, 01-078-0430), carbonates ($CaCO_3$, 01-081-2027), potassium sulphate ($K_2S_4O_6$, 00-002-0441), and aluminosilicates ($(MgAl_2Si_3O_{10})_{0.6}$, 01-073-2337) are identified as a compatible crystalline phases. K-struvite is detected in different 2-Theta degrees, the most significant is located at 20.8° [26]. Although in Fig. 4 the aluminosilicates are not observed, due to the high number of phases, they are derived from the TUN as can be visualised in the SEM-EDS analysis of TUN shown in Fig. 6.

The TG/DTG characterization of the cement at 28 days is shown in

Table 6
Estimated composition of MPC-TUN by means of XRD-TG/DTG.

Compounds	$MgKPO_4$ $(H_2O)_6$	$CaCO_3$	$CaSO_4$	$Mg(OH)_2$	$CaMg_{0.27}Fe_{0.73}$ $(CO_3)_2$	Others
wt%	55.76	4.21	2.51	2.39	1.83	33.3

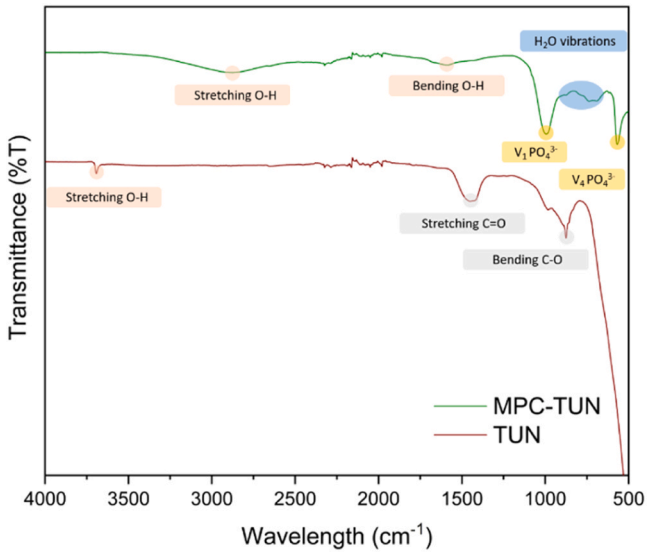

Fig. 10. FT-IR of TUN and MPC-TUN.

Fig. 9. Thermogravimetric analysis confirmed the presence of K-struvite, which has a dehydration temperature from 105 to 136 ºC [27,28]. However, it is possible to identify other non-reactive phases from raw materials. The TG/DTG results revealed the following mass losses and temperature ranges of decomposition: a loss of 22.62 wt% between 25 and 322 °C, attributed to the loss of water from K-struvite; a loss of 0.74 wt% between 322 and 512 °C, attributed to the loss of water from $Mg(OH)_2$ decomposition; and other losses were attributed to the decomposition of carbonates [29,30]. Therefore, the XRD-TG/DTG results show the formation of K-struvite; hence, the MPC was successfully developed. Specifically, the estimated amount of K-struvite in the MPC-TUN is 55.76 wt%, as shown in Table 6. But it also shows the presence of other phases and an increase of the amount of $CaCO_3$ compared to the amount present in TUN, which may be indicative of possible carbonation.

FT-IR spectrum of TUN and MPC-TUN are shown in Fig. 10. On the one hand, TUN spectrum shows the presence of a peak related to the Mg–O vibration (850–600 cm^{-1}) [31]. The peaks around 3700 cm^{-1}, 1450 cm^{-1}, and 870 cm^{-1} are associated with the O–H stretching vibration, with the C═O stretching vibration and with the bending vibration of C–O related to carbonates, respectively [32–34]. The –OH group is attributed to the $Mg(OH)_2$ previously identified in XRD analysis [32]. On the other hand, in the case of MPC-TUN after 28 days of curing, the characteristic bands of K-struvite can be observed in Fig. 10. The phosphate (PO_4^{3-}) peak in K-struvite appears between 1000 and 1200 cm^{-1} [35–37]. Besides, the asymmetrical deformation of PO_4^{3-} is located at 1000 cm^{-1} and the symmetrical one is identified at 575 cm^{-1} [38]. The peaks located around 2900 cm^{-1} and 2300 cm^{-1} are associated to the H–O–H stretching of crystallization water molecules. The peak located around 1700 cm^{-1} corresponds to the H–O–H bending modes of vibrations [33,38]. The Mg–O bond peak is located around 600 cm^{-1} and the vibrations of coordinated water are at 750 cm^{-1} [36,37,39].

Table 7 shows the leaching results and the regulatory limits following the European Commission legislation (Directive 2018/850). Also, the results of the duplicates and the limits are shown in Table 7. The analysis shows that TUN would be accepted in landfills but it would be classified as non-hazardous waste, as Se exceeds the established limit, but the other metal(oid)s are classified as inert waste. In the case of MPC-TUN, after its useful life, it should be managed as hazardous waste, because the Se concentration is quite above the threshold limit. Note that Mo and Sb should be classified as non-hazardous. To reduce the Sb content, a pH reduction would be convenient (around pH=10) to avoid Sb (V) compounds precipitation. It should be noted that the concentrations of all the other metal(oid)s are classified as inert. The trend of increasing concentrations of Mo, Sb, and Se in relation to the raw material has been also observed in other studies involving MPCs developed with various waste and industrial by-products, including LG-MgO [25]. In the coming future, research should be conducted to investigate the internal reaction of these cements and determine the chemical response to this trend.

Fig. 11 shows the different morphology and microstructure of MPC-TUN samples. The surface shows the non-reactive particles are

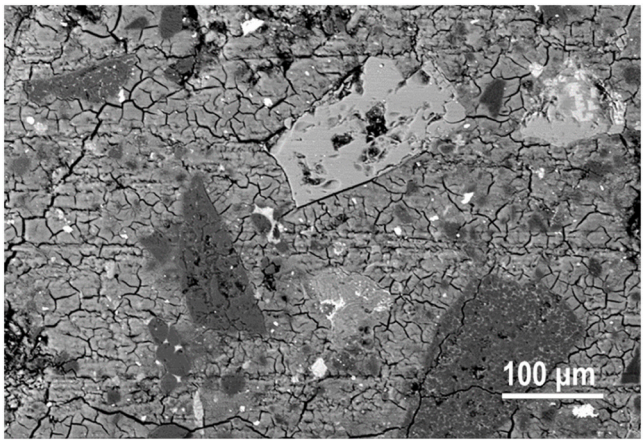

Fig. 11. Backscattered electron micrograph obtained by SEM of MPC formulated with TUN polished sample (x200).

Table 7
Leachates in water following the EN 12457–2 standard.

Sample		mg·kg^{-1}											
	pH	As	Ba	Cd	Cr	Cu	Hg	Mo	Ni	Pb	Sb	Se	Zn
TUN	12.54	< 0.010	2.201	< 0.020	0.019	0.052	< 0.010	0.286	0.032	< 0.050	0.014	0.489	< 0.100
MPC-TUN	11.28	0.411	< 0.050	< 0.020	< 0.050	< 0.050	< 0.010	1.804	< 0.050	< 0.050	0.092	0.989	< 0.100
Limits according to the EN 12457–2													
Inert limit	-	0.5	20	0.04	0.5	2	0.01	0.5	0.4	0.5	0.06	0.1	4
Non-hazardous limit	-	2	100	1	10	50	0.2	10	10	10	0.7	0.5	50
Hazardous limit	-	25	300	5	70	100	2	30	40	50	5	7	200

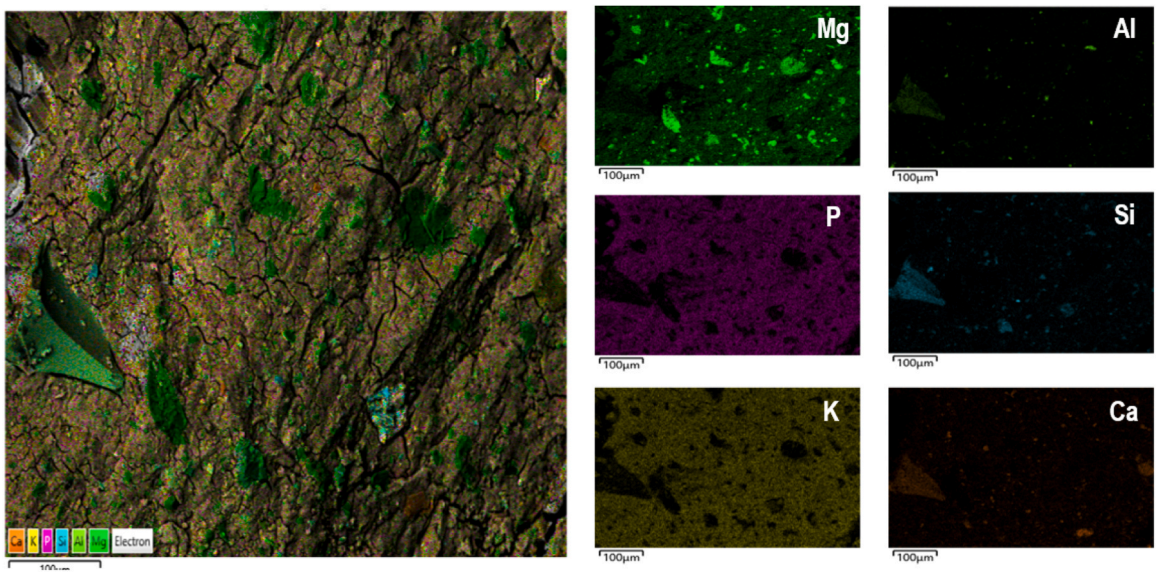

Fig. 12. MPC-TUN SEM-EDS general elemental mapping (left) and the elemental mapping (right) (x200).

embedded in the cementitious matrix. Likewise, the SEM micrograph allows for the observation of microcracking produced by water evaporation during the exothermic setting and curing period. Fig. 12 presents the EDS elemental mapping of MPC-TUN, where the expected elements (Mg, K, P, and O) are observed. Therefore, it is verified that a differentiated matrix of K-struvite predominates with non-reactive nuclei (as can be seen with the green, violet, and yellow colours that refer to magnesium, phosphorus, and potassium, respectively) [29]. Therefore, it is possible to identify the cementitious matrix with the representative morphology of K-struvite by embedding the non-reactive phases from the TUN providing adequate cohesion. On the left side of the Fig. 12, is possible to see a non-reactive particle which is assigned to calcium aluminosilicate particle.

4. Conclusions

In this study, an experimental investigation of MPC-TUN is developed. The results verify that is feasible to formulate MPC-TUN using TUN as raw material. This implies the valorisation of the waste contributes to the evaluation of a potential method for its recovery and reduces its shipment to landfill. Therefore, this valorization can contribute to the sustainability of the planet and promote a future, with a smaller environmental footprint, following the goals of sustainable development.

The results of the study show that TUN is a magnesium oxide-rich waste with adequate reactivity for developing MPC. Therefore, it is a suitable residue for its use as a source of MgO. It is important to highlight that the use of TUN instead of pure MgO promotes the circular economy by reducing CO_2 emissions. Furthermore, K-struvite is successfully obtained using TUN as raw material. Subsequently, it is possible to confirm the correct formulation of an MPC. The microstructure analyses evidence that the main product is the K-struvite matrix, although other non-reactive phases from TUN are identified in the cementitious matrix.

Finally, it is crucial to emphasize that the present study opens up an opportunity to formulate a new alternative cement that can be utilized in various applications within the field of construction. Moreover, the CS performance (~27 MPa at 28 days) suggests its potential use for applications such as cobblestones and street furniture, among other prefabricated materials. In addition, after its service life could be accepted in landfills classified as hazardous waste. Future investigations should be focused on the durability study and the life cycle assessment (LCA) of the MPC-TUN to verify its potential application.

Funding

This work is supported by the Spanish Government with the Grant PID2021-125810OB-C21 funded by MCIN/AEI/10.13039/501100011033 and by "ERDF A way of making Europe". Furthermore, the Agència de Gestió d'Ajuts Universitaris i de Recerca (AGAUR) contributed through Ms A. Alfocea-Roig's PhD grant (FI-DGR 2021). This work is also partially supported by Magnesitas Navarras, S.A. (FBG312160).

CRediT authorship contribution statement

A. Alfocea-Roig: Data curation, Formal analysis, Investigation, Writing - original draft. **S. Huete-Hernández**: Conceptualization, Resources, Visualization, Investigation, Writing - review & editing. **Í .X. García-Zubiri**: Resources, Visualization, Writing - review & editing. **J. Giro-Paloma**: Conceptualization, Visualization, Supervision, Writing - review & editing. **J. Formosa**: Conceptualization, Visualization, Supervision, Methodology, Writing - review & editing, Funding acquisition.

Declaration of Competing Interest

The authors declare that they have no known competing financial interests or personal relationships that could have appeared to influence the work reported in this paper.

Data availability

Data will be made available on request.

Acknowledgments

The authors would like to thank Magnesitas Navarras, S.A. company for material supply. Dr. Jessica Giro-Paloma is a Serra Húnter Fellow. The authors would like to thank the Catalan Government for the quality accreditation given to their research group DIOPMA (2017 SGR 0118, 2021 SGR 00708). DIOPMA is a certified agent TECNIO in the category of technology developers from the Government of Catalonia.

References

[1] 5REFRACT, Systematic and integral valorization of refractories under the "5R" approach, 2018. ⟨http://www.conama.org/conama/download/files/conama2018/CT2018/1222224770.pdf⟩.

[2] F. Mora, Revestimiento refractario en horno de solera galopante, Universidad Carlos III de Madrid (UC3M), 2008. ⟨http://hdl.handle.net/10016/10746⟩.

[3] D. Mazumdar, Review, analysis, and modeling of continuous casting tundish systems, Steel Res. Int. 90 (2019) 1–14, https://doi.org/10.1002/srin.201800279.

[4] D. Blengini Gian Andrea, El. Latunussa Cynthia, Eynard Umberto, Torres De. Matos Cristina, Wittmer Dominic, Georgitzikis Konstantinos, Pavel Claudiu, Carrara Samuel, Mancini Lucia, Unguru Manuela, Blagoeva Darina, Mathieux Fabrice Pennington, Study on the EU's list of Critical Raw Materials (2020), Eur. Com. (2020), https://doi.org/10.2873/867993.

[5] J. Madías, Reciclado de materiales refractarios utilizados en la siderurgia, Acero Lat. (2010) 46–55. ⟨https://www.academia.edu/31032934/Reciclado_de_materiales_refractarios_utilizados_en_la_siderurgia⟩.

[6] M. Musmeci, N.M. Rendtorff, L. Musante, L. Martorello, Characterization of MgO-based tundish working lining materials, microstructure and properties, Ceram. Int. 40 (2014) 14091–14098, https://doi.org/10.1016/j.ceramint.2014.05.138.

[7] EU project REFRASORT, How to turn refractory waste back into raw materials, Innov. Sep. Technol. High Grade Recycl. Refract. Waste Using Non Destr. Technol. (2016). ⟨https://cordis.europa.eu/article/id/197342-how-to-turn-refractory-waste-back-into-raw-materials/es⟩.

[8] THE COUNCIL OF THE EUROPEAN UNION, Directive 1999/31/EC on the landfill of waste, (1999).

[9] THE COUNCIL OF THE EUROPEAN UNION, Directive 2008/98/EC on waste, (2008) 3–30.

[10] R. Maddalena, J.J. Roberts, A. Hamilton, Can Portland cement be replaced by low-carbon alternative materials? A study on the thermal properties and carbon emissions of innovative cements, J. Clean. Prod. 186 (2018) 933–942, https://doi.org/10.1016/j.jclepro.2018.02.138.

[11] A. Naqi, J.G. Jang, Recent Progress in green cement technology utilizing low-carbon emission fuels and raw materials: a review, Sustainability 2 (2019), https://doi.org/10.3390/su11020537.

[12] U. Nations, Sustainable Development Goals, 17 Goals to Transform Our World. (2015). ⟨https://www.un.org/sustainabledevelopment/⟩.

[13] B. Xiao, Y. Chen, Q. Fang, Z. Ding, Research progresses on magnesium phosphate cement-based composites: a review, Gongneng Cailiao/J. Funct. Mater. 51 (2020) 885–898, https://doi.org/10.3969/j.issn.1001-9731.2020.08.002.

[14] S.A. Walling, J.L. Provis, Magnesia-based cements: a journey of 150 years, and cements for the future? Chem. Rev. 116 (2016) 4170–4204, https://doi.org/10.1021/acs.chemrev.5b00463.

[15] M. Le Rouzic, T. Chaussadent, G. Platret, L. Stefan, Mechanisms of k-struvite formation in magnesium phosphate cements, Cem. Concr. Res. 91 (2017) 117–122, https://doi.org/10.1016/j.cemconres.2016.11.008.

[16] Y. Liu, Z. Qin, B. Chen, Experimental research on magnesium phosphate cements modified by red mud, Constr. Build. Mater. 231 (2020), https://doi.org/10.1016/j.conbuildmat.2019.117131.

[17] S. Huete-Hernández, A. Maldonado-Alameda, J. Giro-Paloma, J.M. Chimenos, J. Formosa, Fabrication of sustainable magnesium phosphate cement micromortar using design of experiments statistical modelling: Valorization of ceramic-stone-porcelain containing waste as filler, Ceram. Int. 47 (2021) 10905–10917, https://doi.org/10.1016/j.ceramint.2020.12.210.

[18] M. Riaz, B. Chen, J. Yu, A comprehensive study of basalt fiber reinforced magnesium phosphate cement incorporating ultra fine fly ash, Composites 168 (2019) 204–217, https://doi.org/10.1016/j.compositesb.2018.12.065.

[19] M.A. Haque, B. Chen, Research progresses on magnesium phosphate cement: a review, Constr. Build. Mater. 211 (2019) 885–898, https://doi.org/10.1016/j.conbuildmat.2019.03.304.

[20] Y. Su, J. Yang, D. Liu, S. Zhen, N. Lin, Y. Zhou, Effects of municipal solid waste incineration fly ash on solidification/stabilization of Cd and Pb by magnesium potassium phosphate cement, J. Environ. Chem. Eng. 4 (2016) 259–265, https://doi.org/10.1016/j.jece.2015.11.025.

[21] GCCA, Global Cement and Concrete Association, GCCA 2050 Cem. Concr. Ind. Roadmap Net Zero Concr. (2021). ⟨https://gccassociation.org/concretefuture/⟩.

[22] L.P. Iñigo X. García-Zubiri, Mikel Arandigoyen, Roiner Racedo, Presen Amezketa, Marcelo Lagier, Luciano Disante, Mariano Comas, Silvia Murialdo, Coldmag ®, the easy way to cast, in: Jorn. Mater. Refract. '11 - Refract. Mater. Semin. '11 IAS, 2011, Rosario, Santa Fe, Argentina., 2011. ⟨https://www.magnesitasnavarras.es/wp-content/uploads/coldmag_paper_english.pdf⟩.

[23] J. Formosa, J.M. Chimenos, A.M. Lacasta, M. Niubó, Interaction between low-grade magnesium oxide and boric acid in chemically bonded phosphate ceramics formulation, Ceram. Int. 38 (2012) 2483–2493, https://doi.org/10.1016/j.ceramint.2011.11.017.

[24] A. Maldonado-Alameda, A.M. Lacasta, J. Giro-Paloma, J.M. Chimenos, L. Haurie, J. Formosa, Magnesium phosphate cements formulated with low grade magnesium oxide incorporating phase change materials for thermal energy storage, Constr. Build. Mater. 155 (2017) 209–216, https://doi.org/10.1016/j.conbuildmat.2017.07.227.

[25] S. Huete-Hernández, A. Maldonado-Alameda, A. Alfocea-Roig, J. Giro-Paloma, J. M. Chimenos, J. Formosa, Sustainable magnesium phosphate micromortars formulated with PAVAL® alumina by-product as micro-aggregate, Bol. La Soc. Esp. Ceram. Y. Vidr. (2023) 1–15, https://doi.org/10.1016/j.bsecv.2023.02.001.

[26] Y.J. Du, M.L. Wei, K.R. Reddy, F. Jin, H.L. Wu, Z.Bin Liu, New phosphate-based binder for stabilization of soils contaminated with heavy metals: leaching, strength and microstructure characterization, J. Environ. Manag. 146 (2014) 179–188, https://doi.org/10.1016/j.jenvman.2014.07.035.

[27] H. Lahalle, C. Patapy, M. Glid, G. Renaudin, M. Cyr, Microstructural evolution/durability of magnesium phosphate cement paste over time in neutral and basic environments, Cem. Concr. Res. 122 (2019) 42–58, https://doi.org/10.1016/j.cemconres.2019.04.011.

[28] B. Xu, B. Lothenbach, A. Leemann, F. Winnefeld, Reaction mechanism of magnesium potassium phosphate cement with high magnesium-to-phosphate ratio, Cem. Concr. Res. 108 (2018) 140–151, https://doi.org/10.1016/j.cemconres.2018.03.013.

[29] O. Mgkpo, L.J. Gardner, S.A. Walling, S.M. Lawson, S. Sun, S.A. Bernal, C. L. Corkhill, J.L. Provis, D.C. Apperley, D. Iuga, J.V. Hanna, N.C. Hyatt, Characterization of and Structural Insight into Struvite-K, Inorg. Chem. 4 (2021).

[30] D. Dollimore, S. Lerdkanchanaporn, Thermal Analysis, William Andrew Publishing/Noyes Publications, 1998, https://doi.org/10.1021/a19800038.

[31] G. Balakrishnan, R. Velavan, K. Mujasam Batoo, E.H. Raslan, Microstructure, optical and photocatalytic properties of MgO nanoparticles, Results Phys. 16 (2020), 103013, https://doi.org/10.1016/j.rinp.2020.103013.

[32] M.H. Zahir, M.M. Rahman, K. Irshad, M.M. Rahman, Shape-stabilized phase change materials for solar energy storage: MgO and $Mg(OH)_2$ mixed with polyethylene glycol, Nanomaterials 9 (2019) 1–21, https://doi.org/10.3390/nano9121773.

[33] Y. Yuanquan, Z. Guanhua, G. Jinbo, Q. Dingwen, L. Runqing, An insight into the thermal properties of struvite-k by Rietveld refinement method, J. Mater. Res. Technol. 24 (2023) 3683–3690, https://doi.org/10.1016/j.jmrt.2023.04.032.

[34] P. Makreski, G. Jovanovski, Minerals from Macedonia. Distinction between some rhombohedral carbonates by FT-IR spectroscopy, Bull. Chem. Technol. Maced. (2003).

[35] V.B. Suryawanshi, R.T. Chaudhari, Synthesis and Characterization of Struvite-k Crystals by Agar Gel, J. Cryst. Process Technol. 04 (2014) 212–224, https://doi.org/10.4236/jcpt.2014.44026.

[36] A. Siciliano, C. Limonti, Is K-Struvite precipitation a plausible nutrient recovery method from potassium-containing wastes?—A review, Sustainability (2022), https://doi.org/10.3390/su141811680.

[37] P. Zhang, W.P. Liu, T.L. Zhao, Q.Z. Yao, H. Li, S.Q. Fu, G.T. Zhou, Biomineralization of struvite by Shewanella oneidensis MR-1 for phosphorus recovery: Cr(VI) effect and behavior, J. Environ. Chem. Eng. 10 (2022) 1–9, https://doi.org/10.1016/j.jece.2021.106923.

[38] R.C. de, S. Meira, S.P.A. da Paz, J.A.M. Corrêa, XRD-Rietveld analysis as a tool for monitoring struvite analog precipitation from wastewater: P, Mg, N and K recovery for fertilizer production, J. Mater. Res. Technol. 9 (2020) 15202–15213, https://doi.org/10.1016/j.jmrt.2020.10.082.

[39] N.K. Nga, N.T. Thuy Chau, P.H. Viet, Preparation and characterization of a chitosan/MgO composite for the effective removal of reactive blue 19 dye from aqueous solution, J. Sci. Adv. Mater. Devices 5 (2020) 65–72, https://doi.org/10.1016/j.jsamd.2020.01.009.